Journal of Power Sources 596 (2024) 234033

Contents lists available at ScienceDirect

Journal of Power Sources

journal homepage: www.elsevier.com/locate/jpowsour

Synthesis of organic cathode materials with pyrazine and catechol motifs for rechargeable lithium and zinc batteries

Svit Menart [a,b], Klemen Pirnat [a,*], Andraž Krajnc [a], Francisco Ruiz-Zepeda [a], David Pahovnik [a], John Fredy Vélez Santa [a], Robert Dominko [a,b,c]

[a] National Institute of Chemistry, Ljubljana, Slovenia
[b] Faculty of Chemistry and Chemical Technology, University of Ljubljana, Ljubljana, Slovenia
[c] ALISTORE-European Research Institute, Amiens, France

HIGHLIGHTS

- Organic cathodes.
- Li-battery.
- Zn-battery.
- Pyrazines.
- Quinones.

GRAPHICAL ABSTRACT

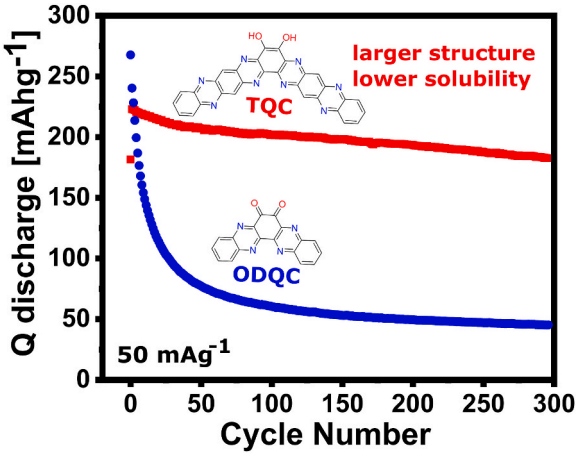

ABSTRACT

Although there are many reports on novel small organic cathode materials for rechargeable lithium and zinc batteries, there is still a lack of materials obtained with a facile synthesis from commercially available precursors, which also exhibit satisfactory cycling stability. Herein, we report a simple synthetic procedure for the simultaneous introduction of carbonyl and pyrazine units into small organic cathode materials. Building on an already known oxidized diquinoxalinecatechol (ODQC) material with cycling stability issues stemming from the dissolution in the electrolyte, we designed an expanded conjugated structure tetraquinoxalinecatechol (TQC). The ODQC shows fast capacity fading in Li-organic batteries having capacity retention of 16.8 % after 300 cycles at a current density of 50 mAg^{-1}. The synthesis of the bigger TQC analog with lower solubility improves cycling stability with a high capacity retention of 82 % after 300 cycles at a current density of 50 mAg^{-1} and a maximum specific capacity of 223 $mAhg^{-1}$ at an average voltage of 2.42 V *vs.* Li/Li^{+}. In Zn-organic battery employing an aqueous electrolyte, TQC delivers a high maximum specific capacity of 301 $mAhg^{-1}$ at 50 mAg^{-1} with an average voltage of 0.76 V, and 71 % capacity retention after 100 cycles.

* Corresponding author.
E-mail address: klemen.pirnat@ki.si (K. Pirnat).

https://doi.org/10.1016/j.jpowsour.2023.234033
Received 21 September 2023; Received in revised form 11 December 2023; Accepted 29 December 2023
Available online 20 January 2024

1. Introduction

Due to ever-increasing demands for efficient energy storage, research is crucial for a new generation of batteries, which are sustainable, low-cost and have increased energy density. Presently used cathodes in commercial lithium-ion batteries possess scarce transition metals, such as Co and Ni. In contrast, organic cathode materials can be made out of abundant raw materials, enabling sustainable production and a lower carbon footprint [1]. Additionally, organic materials possess, flexible structure enabling the accommodation of multivalent cations. Organic cathode materials have been proven to work in aluminium [2,3], magnesium [4,5] and zinc [6,7] batteries. In recent years aqueous zinc-ion batteries have attracted a lot of attention as one of the most promising candidates for large scale energy storage applications. The use of zinc metal offers advantages in terms of low toxicity, low cost, high abundance (Zn resources are at least 20 times higher than Li) and high specific capacity (820 $mAhg^{-1}$) [8–10]. It also enables the use of aqueous electrolytes, which have high ionic conductivity and unlike organic electrolytes do not present a fire hazard [9].

Since the first use of an organic cathode material based on dichloroisocyanuric acid in a lithium primary battery in 1969 [11] several types of organic redox-active materials have been extensively explored, such as carbonyl compounds [7,12], conducting polymers [13,14], stable organic radicals [15,16], organo-sulfur compounds [17,18], and imine compounds [19,20] with comparable or even superior electrochemical performances to conventional inorganic materials. To develop high-energy and high-power-density rechargeable batteries, active materials should possess multiple redox centers and high intrinsic electrical conductivity. Although organic cathode materials already present a sustainable alternative to inorganic materials, there is still a need for new materials obtained with a facile synthesis using readily available precursors.

Recently there have been several reports of small organic cathode materials in lithium and zinc batteries, where the integration of pyrazine and quinone units enabled increased capacity and voltage [21–27]. Small organic cathode materials are known to possess cycling stability issues stemming from their dissolution in the electrolyte [7,28]. Polymerization of the active unit is a commonly used approach to limit the dissolution of the active material in the electrolyte, which can impede active material utilization [12].

Building on an already known oxidized diquinoxalinecatechol (ODQC) material with cycling stability issues stemming from the dissolution in the organic based electrolytes [29], we designed an expanded conjugated structure tetraquinoxalinecatechol (TQC). We hypothesized that the synthesis of a bigger conjugated derivative (TQC) could increase the intermolecular interactions between molecules, thus mitigating the dissolution in the electrolyte. The hypothesis has been confirmed in lithium battery configuration, where TQC exhibited one of the best cycling stabilities of reported small organic cathode materials. On the other hand, the results in the configuration of zinc battery show an opposite trend, with TQC demonstrating faster capacity fading than its smaller ODQC analog.

2. Materials and methods

Material characterization: ^{1}H and ^{13}C NMR spectra were recorded on Avance Neo 600 MHz spectrometer (Bruker) using DMSO-d_6 containing 0.03 wt% tetramethylsilane (TMS). ^{1}H–^{13}C CP-MAS NMR spectra were recorded on Avance Neo 400 MHz spectrometer (Bruker) equipped with a 4 mm CP-MAS probe with ^{1}H–^{19}F and ^{31}P-^{15}N coils. The sample rotation frequency was 10 kHz and relaxation delay set to 2s. Chemical shifts are given in ppm relative to the tetramethyl silane (TMS) standard. FT-IR spectroscopy was recorded in ATR mode on IFS66/S (Bruker) using germanium window in the wavelength range of 600–4000 cm^{-1}. Mass spectrometry measurements were recorded on UltrafleXtreme MALDI-TOF (Bruker Daltonik) mass spectrometers. The samples were first mixed with the matrix dithranol in agate mortar. The solid mixture was then transferred to the MALDI plate using a spatula and the reflective positive ion mode was used to acquire the mass spectra. Calibration was performed externally using a poly(methyl methacrylate) standard (MALDI validation set PMMA, Fluka Analytical). TEM images and spectroscopic data were taken in a Cs corrected STEM JEOL ARM 200 CF analytical instrument operated at 80 kV and equipped with a GIF Quantum (Gatan) Dual EELS (Electron Energy Loss Spectroscopy) spectrometer. TGA measurements were performed on a TGA/DSC 1 thermogravimetric analyzer (Mettled Toledo, Switzerland) at a heating rate of 10 °C min^{-1} from 40 to 800 °C in a nitrogen atmosphere.

Electrochemical measurements: Electrochemical measurements were carried out using potentiostat/galvanostat VMP3 (Bio-Logic, France) at room temperature (25 °C).

Li battery: Working electrode was prepared by mixing 60 wt % of the active material, 30 wt % of Printex XE2 carbon black, and 10 wt % of polytetrafluoroethylene (PTFE) binder (60 wt % water dispersion, Aldrich) in 2-propanol. The mixture was ball milled in a planetary ball mill (Retsch PM100) at 300 rpm for 30 min in ambient atmosphere. Obtained slurry was rolled into a thin film, pressed onto an Al-mesh (mesh size 100) current collector and cut into circular discs (φ = 12 mm), which were afterwards dried at 50 °C for 1 day. Swagelok type battery cells were assembled in an argon filled glovebox (O_2 < 1 ppm, H_2O < 1 ppm) by separating working electrodes and lithium foil discs (φ = 12 mm) with 2 pieces (φ = 13 mm) of Celgard 2320 separators wetted with 3 drops of 1 M LiTFSI in 1:1 (v/v) 1,3-dioxolane(DOL) and 1,2-dimethoxyethane (DME) or 3 drops of LP30 electrolyte.

Zn battery: Working electrode was prepared by mixing 60 wt % of the active material, 30 wt % of Printex XE2 carbon black, and 10 wt % of polytetrafluoroethylene (PTFE) binder (60 wt % water dispersion, Aldrich) in 2-propanol. The mixture was ball milled in a planetary ball mill (Retsch PM100) at 300 rpm for 30 min in ambient atmosphere. Obtained slurry was rolled into a thin film on glass and cut into circular discs (φ = 10 mm), which were afterwards dried at 50 °C for 1 day to obtain free standing electrodes. Swagelok type battery cells were assembled in ambient atmosphere by separating free standing cathode electrodes and zinc foil discs (φ = 10 mm) with 2 pieces (φ = 13 mm) of glass fiber separator (Whatman GF/A) wetted with 3 drops of 3 M $ZnSO_4$. 3 M $ZnSO_4$ electrolyte was prepared by dissolving an appropriate amount of zinc sulfate heptahydrate ($ZnSO_4{\cdot}7H_2O$) in water.

Computational calculations: Density functional theory (DFT) computations were carried out using the B3LYP hybrid density functional with 6-31G* basis set as implemented in Spartan'14 program.

Synthesis of TQC: A mixture of sodium rhodizonate (0.70 g, 3.27 mmol) and 2,3-diaminophenazine (1.58 g, 7.52 mmol) was added to 50 mL of deoxygenated glacial acetic acid and heated at 120 °C for 48 h under inert atmosphere. Upon cooling to room temperature, the solid was filtered and washed with glacial acetic acid, acetone, ethanol and water. The product was additionally purified using 24 h Soxhlet extraction with ethanol. Obtained product was dried at 80 °C overnight yielding crude TQC as a black powder in 98 % yield (yield is based on the formation of pure TQC (**1**)). The end product is a mixture of TQC (**1**) and TQC (**2**), which could not be further purified due to insolubility of the compounds.

^{1}H–^{13}C CP-MAS (ppm): 171.4, 154.0, 141.2, 128.9, 114.3, 104.3.

Mass spectrum (MALDI, *m/z*): $[M+H]^+$ calculated for $C_{30}H_{15}N_8O_2$, 519.1; found, 519.0.

ATR-IR (cm^{-1}): 3160 broad, 1686, 1603, 1582, 1518, 1503, 1475, 1451, 1415, 1394, 1356, 1310, 1299, 1250, 1213, 1153, 1128, 1077, 1043, 958, 917, 873, 862, 844, 796, 752, 655, 617.

Synthesis of DQC, ODQC: See supporting information.

3. Results and discussion

The TQC material was synthesized through a facile condensation

reaction between 2,3-diaminophenazine and sodium rhodizonate in acetic acid with near quantitative yield (Fig. 1a). The commercially available 2,3-diaminophenazine precursor can be efficiently produced with minimal waste from 1,2-phenylenediamine [30]. The extremely low solubility of the compound in the commonly used NMR solvents prevents the characterization with liquid NMR, therefore a solid-state $^{1}H–^{13}C$ CP-MAS NMR was performed. The measurement revealed four main peaks at 104.3, 114.3, 128.9, and 141.2 ppm, corresponding to aromatic carbons in the TQC molecule, and additional peaks at 171.4 ppm and 154.0 ppm, indicating the presence of the carbonyl unit (C═O) in the oxidized form of TQC (Figs. 1b, **2**). Formation of both the oxidized TQC (**2**) and catechol TQC (**1**) forms were also observed in the synthesis of smaller ODQC analog, where a part of the catechol precursor compound (DQC) oxidizes to ODQC during soxhlet purification and drying at 80 °C on air (**S1**). Additionally, the successful synthesis of TQC was confirmed with MALDI-TOF mass spectrometry (Fig. 1c, Fig. S1), where a peak population is observed starting at 519.0 Da, which is in good agreement with the calculated exact mass of 519.1 Da for [TQC (**1**) + H]$^{+}$. The most intensive peak in an expected isotopic pattern for [TQC (**1**) + H]$^{+}$ should be at 519.1 Da, however, there are several additional peaks with higher intensities visible in the spectrum, with masses increasing by 1 Da. They are present due to the laser-induced photoreduction of TQC. Namely, in contrast to the electrospray ionization, the determination of the exact mass of the compound with MALDI-TOF MS could be obscured by the reduction of compounds during the ionization process [31]. Compounds containing quinone [32] and pyrazine [33] motifs were shown to get reduced during MALDI and FAB ionization conditions. Similar to the liquid NMR, the utilization of electrospray ionization (ESI) mass spectrometry did not yield results, presumably due to insufficient solubility. The morphology as can be seen from STEM imaging (Fig. 1d and e) consists of different layers of material in an agglomerated form with some porosity. Overall, a non-ordered structure is identified from the selected area electron diffraction (SAED) pattern (Fig. S2). Edges from carbon (C K), nitrogen (N K) and oxygen (O K) were identified with Electron Energy Loss Spectroscopy (EELS) as shown in Fig. S2.

The synthesis of DQC was done in an analogous way to the synthesis of TQC (Fig. 2a), and DQC was transformed to ODQC with oxidation in nitric acid. The ODQC was soluble in deuterated dimethyl sulfoxide (DMSO-d_6), which enabled the characterization with liquid NMR spectroscopy. ^{1}H NMR spectrum revealed four peaks with equal integral values at 8.45, 8.37, 8.12 and 8.08 ppm corresponding to four

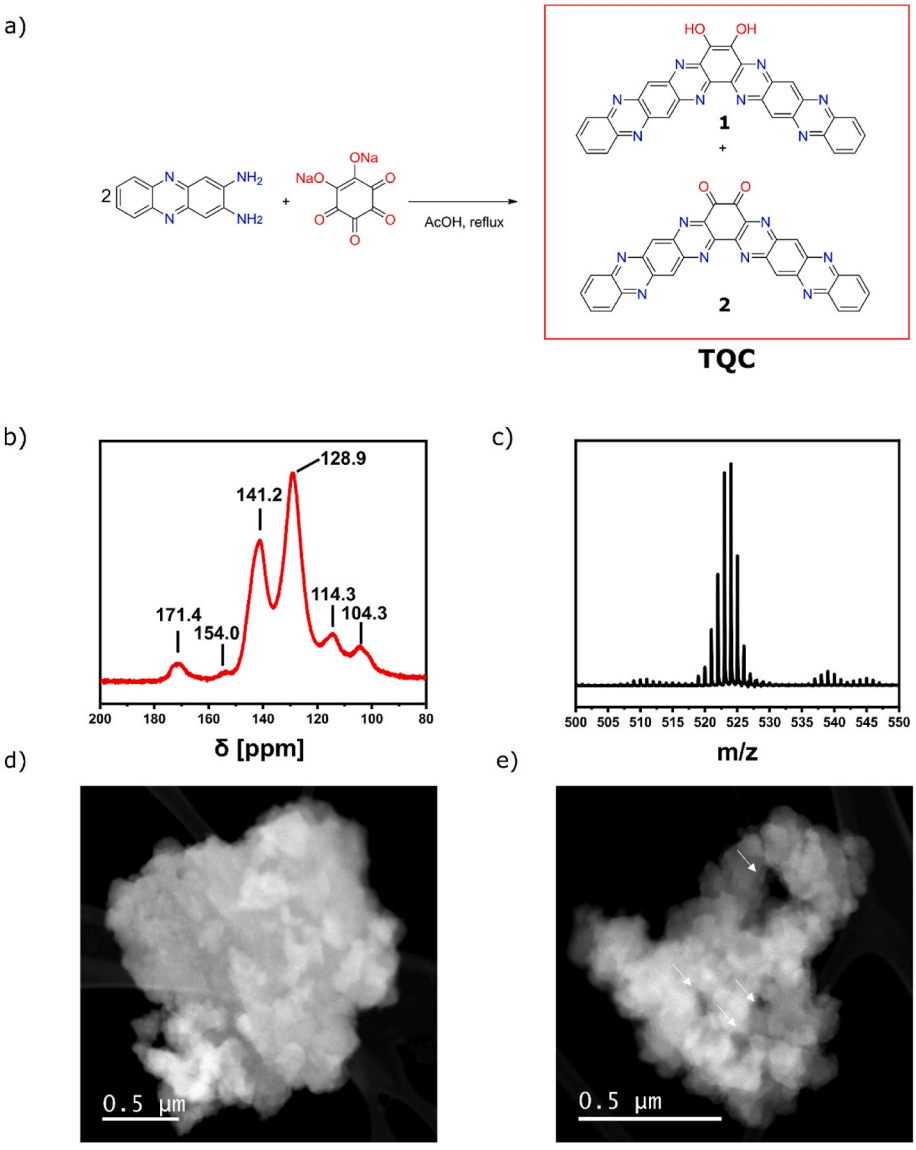

Fig. 1. a) Synthesis of TQC. b) $^{1}H–^{13}C$ CP-MAS NMR spectrum of TQC. c) MALDI-TOF MS spectrum of crude TQC. d) and e) typical morphology and structure of the material imaged by annular dark field (ADF), with white arrows marking holes in the structure.

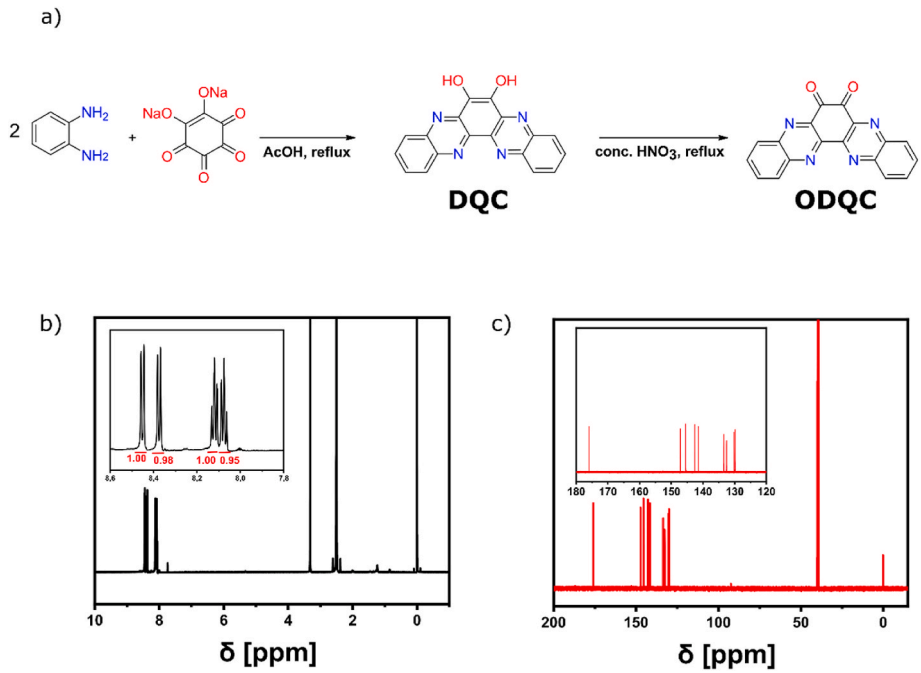

Fig. 2. a) Synthesis of ODQC. b) ^{1}H NMR (DMSO-d_6) spectrum of ODQC with an insert of the zoomed region between 7.8 and 8.6 ppm. c) ^{13}C NMR (DMSO-d_6) spectrum of ODQC with an insert of the zoomed region between 120 and 180 ppm.

distinguishable aromatic protons in ODQC (Fig. 2b). ^{13}C NMR spectrum exhibited nine peaks at 175.8, 147.0, 145.3, 142.5, 141.4, 133.4, 132.5, 130.1 and 129.8 ppm which match with nine types of C atoms in the ODQC molecule (Fig. 2c).

The electrochemical performances of synthesized TQC and ODQC molecules were evaluated in a Swagelok Li-organic battery cell using 1 M lithium bis(trifluoromethanesulfonyl)imide (LiTFSI) in 1:1 (v/v) 1,3-dioxolane (DOL) and 1,2-dimethoxyethane (DME) as an electrolyte in the voltage range of 1.5–3.8 V *vs.* Li/Li^{+}. ODQC has a theoretical capacity of 515 mAhg^{-1} based on a six electron exchange reaction (Fig. 3).

Galvanostatic measurement of ODQC at 50 mAg^{-1} shows three distinct discharge plateaus at around 3.1 V, 2.9 V and 1.8 V. The system reached its highest capacity of 268 mAhg^{-1} in the first discharge with an average voltage of 2.58 V (Fig. 4a). The system exhibited fast capacity fading attributed to the dissolution of the active material in the electrolyte reaching 62.7 % and 16.8 % capacity retention in the 10th and 300th cycle, respectively (Fig. 4b). Full capacity of the material could not be realized due to the decomposition of the ether electrolyte at low potential (Fig. S3a), therefore the material was also evaluated in a commercial LP30 carbonate electrolyte (1 M lithium hexafluorophosphate ($LiPF_6$) in 1:1 (v/v) ethylene carbonate (EC) and dimethyl carbonate (DMC)) with decomposition at lower potential (Fig. S3b). In it, ODQC delivered almost full utilization of redox centers with capacity reaching 484 mAhg^{-1} in the first discharge (Fig. S4a), but similar to the ether electrolyte experienced fast capacity fading (Fig. S4b). Fast capacity fading prevented us to conduct the rate performance test. A comparison of the galvanostatic measurements between ODQC and TQC clearly shows that the problem of solubility of the material in the ether electrolyte was mostly resolved, with TQC demonstrating a high 82.1 % capacity retention after 300 cycles at a low current density of 50 mA g^{-1} making it one of the most stable small organic cathode materials (Fig. 4d). The system reached its highest capacity of 223 mAhg^{-1} in the first cycle with an average voltage of 2.42 V. In contrast to ODQC, the galvanostatic charge/discharge curves of TQC exhibited a sloping curve without distinct plateaus (Fig. 4c). The TQC possesses a theoretical capacity of 310 mAhg^{-1} based on a six electron exchange reaction and 517 mAhg^{-1} based on a ten electron exchange reaction including the outer quinoxaline units. Similar to

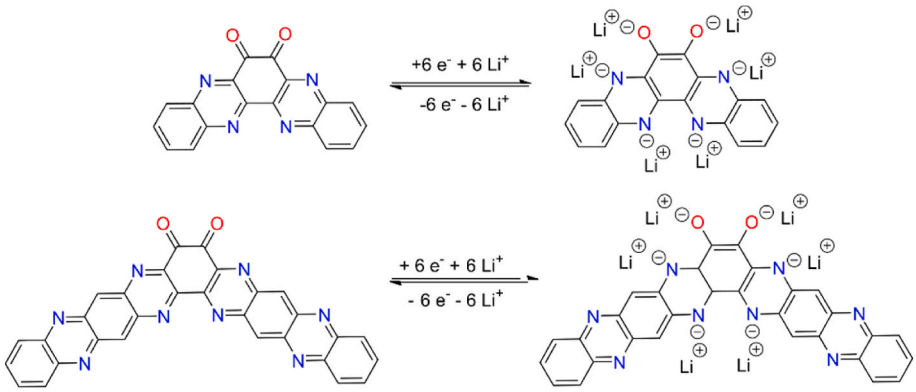

Fig. 3. Proposed redox mechanism of ODQC (up) and TQC (down) based on the literature review of similar reported compounds [22,24,25], assuming complete reduction of inner pyrazine and quinone redox centers. Comment: The redox mechanism of TQC could involve different combinations of inner and outer pyrazine rings. Due to the simplicity the scheme depicts only the reduction of inner redox centers.

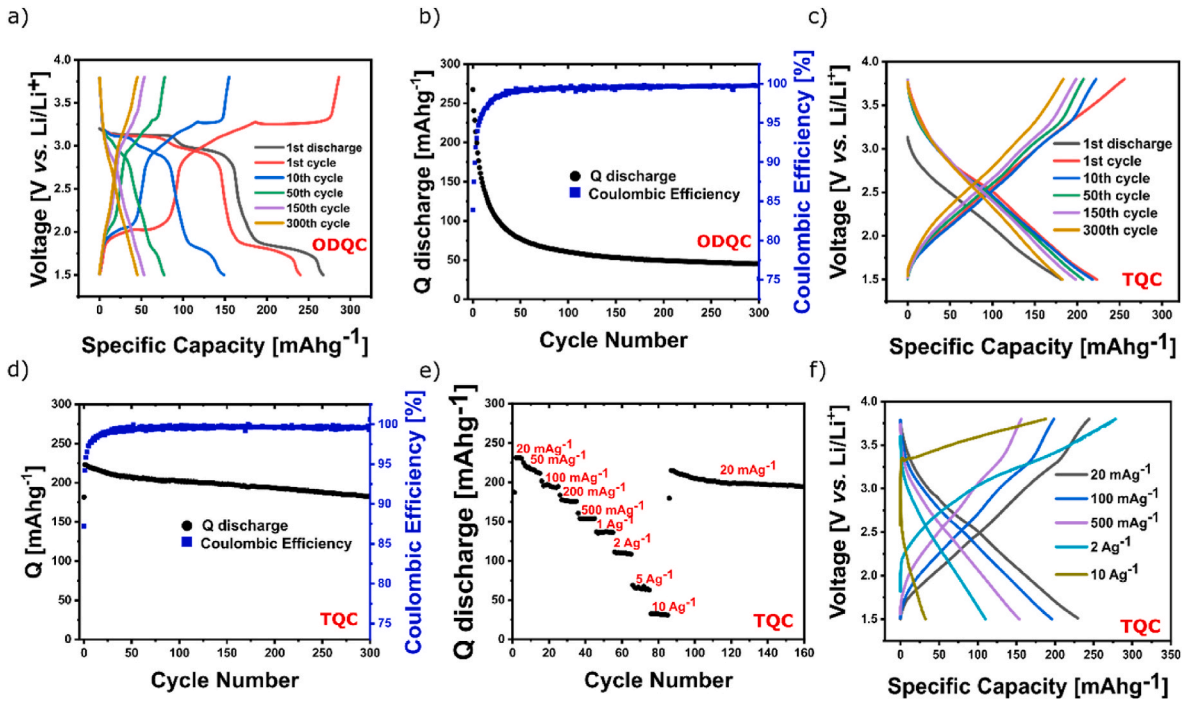

Fig. 4. Li battery: a) Galvanostatic charge/discharge curves of ODQC at 50 mAg^{-1}. b) Cycling stability of ODQC at 50 mAg^{-1}. c) Galvanostatic charge/discharge curves of TQC at 50 mAg^{-1}. d) Cycling stability of TQC at 50 mAg^{-1}. e) Rate performance of TQC. f) Charge/discharge curves of TQC at different current densities obtained from the rate performance test. *All tests were conducted in 1 M LiTFSI in 1:1 (v/v) DOL and DME electrolyte.

ODQC, TQC was also evaluated in commercial LP30 electrolyte, where it achieved almost complete utilization of inner redox active centers reaching a maximum capacity of 291 $mAhg^{-1}$ in second cycle (Fig. S5a). On the other hand, the use of carbonate electrolyte sacrificed the stability of the material showing fast capacity fading (Fig. S5b). Although the molecular structure was expanded with an additional redox active quinoxaline unit, we presume, that the full capacity could not be realized due to the redox activity of quinoxaline units lying even below the stability window of the LP30 electrolyte [34]. The high cycling stability of TQC enabled to carry out rate performance test, where the material reached a capacity of 66 $mAhg^{-1}$ (29 % of the maximum capacity) at a current density of 5 Ag^{-1} (Fig. 4e).

The electrochemical performance of synthesized TQC and ODQC molecules was evaluated in a Swagelok Zn-organic battery cell using an aqueous solution of 3 M $ZnSO_4$ as an electrolyte in the voltage window of 0.25–1.6 V *vs.* Zn/Zn^{2+}. We have checked that this potential window lies inside electrolyte stability window (Fig. S7a). Galvanostatic measurements of ODQC show slow activation with a gradual increase of capacity reaching a maximum value of 157 $mAhg^{-1}$ at 50 mAg^{-1} in the 70th cycle with an average discharge voltage of 0.56 V (Fig. 5a). The discharge curve exhibits two plateaus, a less pronounced sloping plateau at around 1.2 V and a distinct plateau at around 0.5 V (Fig. 5b). In contrast with the lithium system, the cycling stability in the zinc system possesses much better performance reaching 86 % capacity retention in 130 cycles after the activation period. Better cycling stability could be attributed to the lower solubility of the material and its discharged products in the aqueous electrolyte. A rate performance test was conducted after the 30 cycles of the activation period. The system delivered a capacity of 45 $mAhg^{-1}$ (28 % of maximum capacity) at the highest current of 5 Ag^{-1} (Fig. 5c and d).

The discharge curves of TQC displayed two less distinct sloping plateaus at around 1.1 V and 0.5 V (Fig. 5e). The system reached the maximum capacity of 301 $mAhg^{-1}$ at 50 mAg^{-1} with an average voltage of 0.76 V. The TQCs capacity retention is 71 % after 100 cycles (Fig. 5f). In contrast to the lithium system, the rate performance of TQC in the Zn battery did not show overcharging at higher currents (Fig. 5h). At the highest current of 10 Ag^{-1} the system reached a capacity of 114 $mAhg^{-1}$ (38 % of the maximum capacity) (Fig. 5g). The comparison of electronic structures of ODQC and TQC obtained with the use of the density functional theory (DFT) computational method, shows a substantial difference between the energy gap of HOMO and LUMO orbital (3.33 eV *vs.* 2.19 eV *vs.* 2.26 eV for ODQC, TQC (**1**) and TQC (**2**), respectively) suggesting possible higher intrinsic electronic conductivity of TQC (Fig. S8). Moreover, the obtained DFT results correlate well with the observed difference in the initial voltage drop measured during the start of the discharge step (0.39 V *vs.* 0.26 V, for ODQC and TQC, respectively). The voltage drop was attained from the voltage curves of the rate performance test at 2 Ag^{-1} (Fig. S9). In general the magnitude of the initial voltage drop (read out as the extrapolated Ohmic drop, ΔV, Fig. S9) at the reversal of current is proportional to the sum of resistances of bulk electrolyte (in separator) plus the resistance of electron wiring (resistance along carbon black matrix and all the electron contact resistances). In fact, due to the current reversal at the switch from charge to discharge direction the read out value of ΔV corresponds to 2 × Ohmic resistance. Accordingly, for similar electrode thicknesses and the same electrode composition (similar packing of active material and conductive additive) and for the same type of electrolyte the change of the value of ΔV (at the same current density) can serve as an approximate measure for the change of the electron wiring resistance of the electrode composite [35]. We presume that the latter is directly affected by the quality of contact between carbon black and active material and so it is typically improved when the intrinsic conductivity of the active material is higher (considering similar effective contacting area). Thus the combined results of ΔV determination and found lower energy gap of TQC material suggest that the observed better rate performance in comparison with ODQC is (at least partially) due to its higher electronic conductivity. Stationary grid storage requires the utilization of moderate cycling rates between 0.25C and 2 C [8]. Many reports of organic cathode materials show cycling at rates as high as 1000 C, which can mask the instability of the materials and is of limited importance for grid storage. Cycling of the TQC at a higher current of 500 mAg^{-1} (≈1.7C cycling rate) showed capacity retention of 88 % after 100 cycles

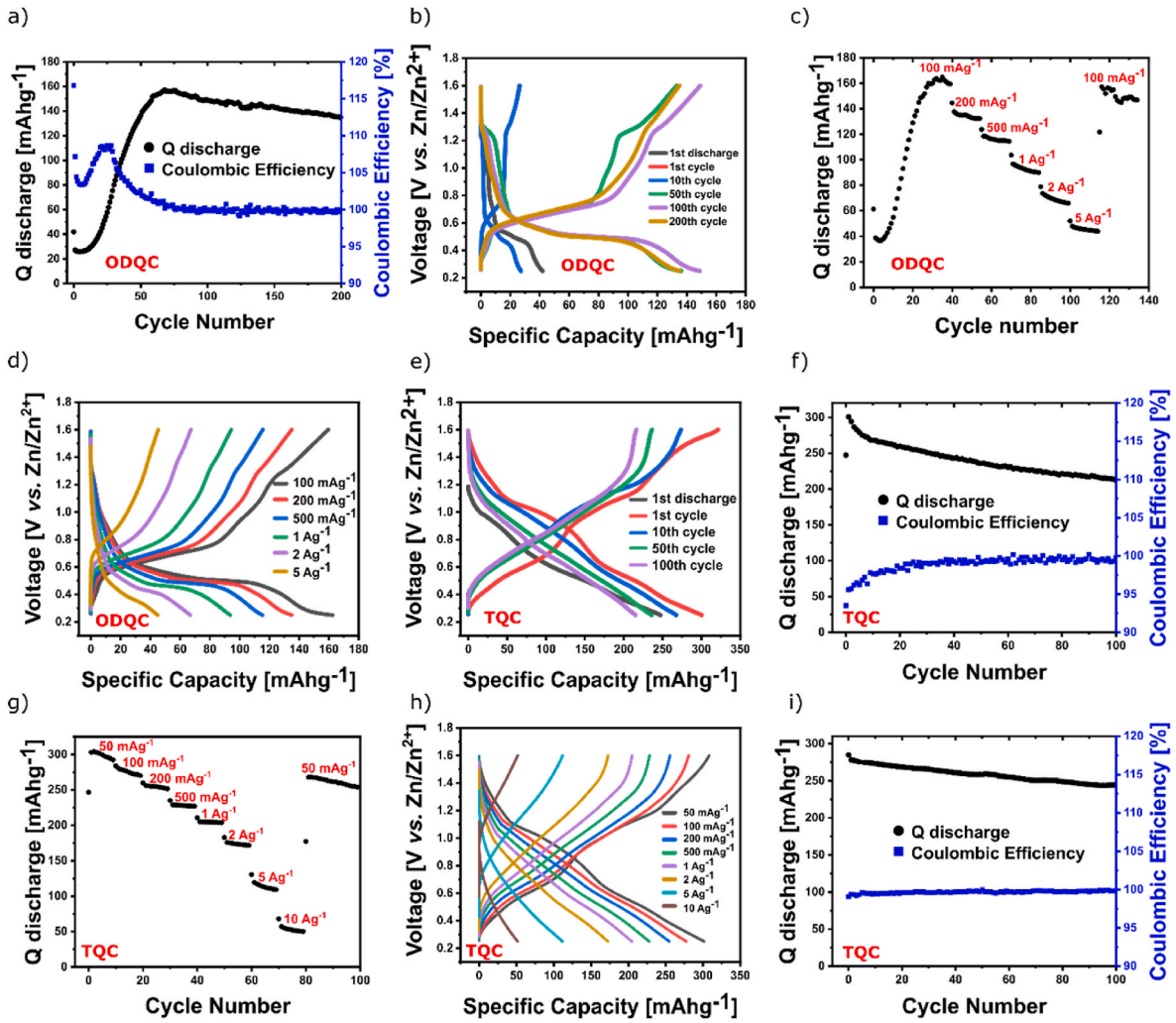

Fig. 5. Zn battery a) Galvanostatic charge/discharge curves of ODQC at 50 mAg^{-1}. b) Cycling stability of ODQC at 50 mAg^{-1}. c) Rate performance of ODQC. d) Charge/discharge curves of ODQC at different current densities obtained from the rate performance test. e) Galvanostatic charge/discharge curves of TQC at 50 mAg^{-1}. f) Cycling stability of TQC at 50 mAg^{-1}. g) Rate performance of TQC. h) Charge/discharge curves of TQC at different current densities obtained from the rate performance test. i) Cycling stability of TQC at 500 mAg^{-1}.

(Fig. 5i).

4. Conclusion

In summary, we presented a facile synthesis strategy for the simultaneous incorporation of pyrazine and catechol units into organic cathode materials. Newly synthesized TQC material demonstrated one of the best cycling stabilities of small organic cathode materials in Li-organic batteries with capacity retention of 82.1 % after 300 cycles at a low current of 50 mAg^{-1}. Smaller analogue ODQC exhibited a higher initial capacity of 268 $mAhg^{-1}$ but had worse cycling stability (16.8 % capacity retention after 300 cycles at 50 mAg^{-1}) attributed to the dissolution of the active material in the electrolyte. The materials were also evaluated in Zn-organic battery where TQC exhibited a high initial capacity of 301 $mAhg^{-1}$ and showed moderate cycling stability (71 % capacity retention after 100 cycles at 50 mAg^{-1}). ODQC experienced a slow activation step reaching the highest capacity of 157 $mAhg^{-1}$ in the 70th cycle and showed better cycling stability (89 % capacity retention after 100 cycles at 50 mAg^{-1}) than TQC. Our hypothesis that the synthesis of a bigger TQC analog could solve cycling stability issues has been confirmed for Li battery, while worse performance in the Zn battery could possibly be associated with higher solubility of salt-like discharge products in the aqueous electrolyte. We believe that the simplicity of the synthesis enables its widespread use for the development of new organic cathode materials.

CRediT authorship contribution statement

Svit Menart: Conceptualization, Data curation, Formal analysis, Investigation, Methodology, Resources, Visualization, Writing – original draft, Writing – review & editing. **Klemen Pirnat:** Formal analysis, Funding acquisition, Resources, Supervision, Writing – review & editing. **Andraž Krajnc:** Formal analysis, Investigation, Methodology, Resources, Visualization, Writing – review & editing. **Francisco Ruiz-Zepeda:** Formal analysis, Investigation, Methodology, Resources, Visualization, Writing – review & editing. **David Pahovnik:** Formal analysis, Investigation, Methodology, Resources, Visualization, Writing – review & editing. **John Fredy Vélez Santa:** Conceptualization, Formal analysis, Investigation, Methodology, Resources, Supervision, Visualization, Writing – review & editing. **Robert Dominko:** Funding acquisition, Project administration, Resources, Writing – review & editing.

Declaration of competing interest

The authors declare that they have no known competing financial interests or personal relationships that could have appeared to influence

the work reported in this paper.

Data availability

Data will be made available on request.

Acknowledgments

The authors acknowledge the financial support from the Slovenian Research Agency young researcher scheme, ARRS research projects N2-0214 and N2-0165, research programs P2-0423 and P2-0145, Ministry of Education, Science and Sport (MIZS) for funding M. Era-net project InsBioration (call 2021) and Honda R&D Germany. We would also like to acknowledge fruitful discussion with Jože Moškon.

Appendix A. Supplementary data

Supplementary data to this article can be found online at https://doi.org/10.1016/j.jpowsour.2023.234033.

References

[1] Y. Lu, J. Chen, Prospects of organic electrode materials for practical lithium batteries, Nat. Rev. Chem 4 (2020) 127–142.
[2] J. Bitenc, N. Lindahl, A. Vizintin, M.E. Abdelhamid, R. Dominko, P. Johansson, Concept and electrochemical mechanism of an Al metal anode – organic cathode battery, Energy Storage Mater. 24 (2020) 379–383.
[3] X. Peng, Y. Xie, A. Baktash, J. Tang, T. Lin, X. Huang, Y. Hu, Z. Jia, D.J. Searles, Y. Yamauchi, L. Wang, B. Luo, Heterocyclic conjugated polymer nanoarchitectonics with synergistic redox-active sites for high-performance aluminium organic batteries, Angew. Chem. Int. Ed. 61 (2022) e202203646.
[4] A. Vizintin, J. Bitenc, A. Kopač Lautar, J. Grdadolnik, A. Randon Vitanova, K. Pirnat, Redox mechanisms in Li and Mg batteries containing poly(phenanthrene quinone)/graphene cathodes using operando ATR-IR spectroscopy, ChemSusChem 13 (2020) 2328–2336.
[5] T. Bančič, J. Bitenc, K. Pirnat, A. Kopač Lautar, J. Grdadolnik, A. Randon Vitanova, R. Dominko, Electrochemical performance and redox mechanism of naphthalene-hydrazine diimide polymer as a cathode in magnesium battery, J. Power Sources 395 (2018) 25–30.
[6] S. Zheng, Q. Wang, Y. Hou, L. Li, Z. Tao, Recent progress and strategies toward high performance zinc-organic batteries, J. Energy Chem. 63 (2021) 87–112.
[7] Q. Zhao, W. Huang, Z. Luo, L. Liu, Y. Lu, Y. Li, L. Li, J. Hu, H. Ma, J. Chen, High-capacity aqueous zinc batteries using sustainable quinone electrodes, Sci. Adv. 4 (2018).
[8] C. Li, S. Jin, L.A. Archer, L.F. Nazar, Toward practical aqueous zinc-ion batteries for electrochemical energy storage, Joule 6 (2022) 1733–1738.
[9] B. Tang, L. Shan, S. Liang, J. Zhou, Issues and opportunities facing aqueous zinc-ion batteries, Energy Environ. Sci. 12 (2019) 3288–3304.
[10] L. Hu, P. Xiao, L. Xue, H. Li, T. Zhai, The rising zinc anodes for high-energy aqueous batteries, Inside Energy 3 (2021) 100052.
[11] D.L. Williams, J.J. Byrne, J.S. Driscoll, High energy density lithium/dichloroisocyanuric acid battery system, Electrochem. Soc. J. 116 (1969) 2–4.
[12] K. Pirnat, J. Bitenc, A. Vizintin, A. Krajnc, E. Tchernychova, Indirect synthesis route toward cross-coupled polymers for high voltage organic positive electrodes, Chem. Mater. 30 (2018) 5726–5732.
[13] L.M. Zhu, A.W. Lei, Y.L. Cao, X.P. Ai, H.X. Yang, An all-organic rechargeable battery using bipolar polyparaphenylene as a redox-active cathode and anode, Chem. Commun. 49 (2013) 567–569.
[14] Y.-J. Ye, K. uan Liu, Y. Song, Xiaoqi Sun, Y. J Ye, D.S. ong, A long-cycle-life self-doped polyaniline cathode for rechargeable aqueous zinc batteries, Angew. Chem. 130 (2018) 16597–16601.
[15] C. Friebe, U.S. Schubert, High-power-density organic radical batteries, Top. Curr. Chem. 375 (2017) 1–35.
[16] E. Schröter, L. Elbinger, M. Mignon, C. Friebe, J.C. Brendel, M.D. Hager, U. S. Schubert, High-capacity semi-organic polymer batteries: from monomer to battery in an all-aqueous process, J. Power Sources 556 (2023) 232293.
[17] P. Hu, X. He, M. Ng, J. Ye, C. Zhao, S. Wang, K. Tan, A. Chaturvedi, H. Jiang, C. Kloc, W. Hu, Y. Long, Trisulfide-bond acenes for organic batteries, Angew. Chem. Int. Ed. 58 (2019) 13513–13521.
[18] M.R. Tuttle, C. Walter, E. Brackman, C.E. Moore, M. Espe, C. Rasik, P. Adams, S. Zhang, Redox-active zinc thiolates for low-cost aqueous rechargeable Zn-ion batteries, Chem. Sci. 12 (2021) 15253–15262.
[19] J. Zhao, J. Yang, P. Sun, Y. Xu, Sodium sulfonate groups substituted anthraquinone as an organic cathode for potassium batteries, Electrochem. Commun. 86 (2018) 34–37.
[20] Z. Tie, L. Liu, S. Deng, D. Zhao, Z. Niu, Proton insertion chemistry of a zinc–organic battery, Angew. Chem. Int. Ed. 59 (2020) 4920–4924.
[21] S. Menart, K. Pirnat, D. Pahovnik, R. Dominko, Triquinoxalinediol as organic cathode material for rechargeable aqueous zinc-ion batteries, J. Mater. Chem. A 11 (2023) 10874–10882.
[22] A. Shimizu, Y. Tsujii, H. Kuramoto, T. Nokami, Y. Inatomi, N. Hojo, J. Yoshida, Nitrogen-containing polycyclic quinones as cathode materials for lithium-ion batteries with increased voltage, Energy Technol. 2 (2014) 155–158.
[23] T. Shi, G. Li, Y. Han, Y. Gao, F. Wang, Z. Hu, T. Cai, J. Chu, Z. Song, Oxidized indanthrone as a cost-effective and high-performance organic cathode material for rechargeable lithium batteries, Energy Storage Mater. 50 (2022) 265–273.
[24] M. Wu, N.T.H. Luu, T. Chen, H. Lyu, T. Huang, S. Dai, X. Sun, A.S. Ivanov, J. Lee, I. Popovs, W. Kaveevivitchai, Supramolecular self-assembled multi-electron-acceptor organic molecule as high-performance cathode material for Li-ion batteries, Adv. Energy Mater. 11 (2021) 2100330.
[25] Z. Chen, J. Wang, T. Cai, Z. Hu, J. Chu, F. Wang, X. Gan, Z. Song, Constructing extended π-conjugated molecules with o-quinone groups as high-energy organic cathode materials, ACS Appl. Mater. Interfaces 14 (2022) 27994–28003.
[26] Y. Gao, G. Li, F. Wang, J. Chu, P. Yu, B. Wang, H. Zhan, Z. Song, A high-performance aqueous rechargeable zinc battery based on organic cathode integrating quinone and pyrazine, Energy Storage Mater. 40 (2021) 31–40.
[27] L. Lin, Z. Lin, J. Zhu, K. Wang, W. Wu, T. Qiu, X. Sun, A semi-conductive organic cathode material enabled by extended conjugation for rechargeable aqueous zinc batteries, Energy Environ. Sci. 16 (2023) 89–96.
[28] X. Liu, Z. Ye, Nitroaromatics as high-energy organic cathode materials for rechargeable alkali-ion (Li^+, Na^+, and K^+) batteries, Adv. Energy Mater. 11 (2021) 2003281.
[29] I. Masato, C. Kuniko, N. Kosuke, K. Yusuke, O. Shigeto, N. Hideo, Electrode Active Material, WO2015147326A1.
[30] F. Ferlin, P.M. Luque Navarro, Y. Gu, D. Lanari, L. Vaccaro, Waste minimized synthesis of pharmaceutically active compounds: via heterogeneous manganese catalysed C-H oxidation in flow, Green Chem. 22 (2020) 397–403.
[31] S. Okuno, M. Nakano, G.E. Matsubayashi, R. Arakawa, Y. Wada, Reduction of organic dyes in matrix-assisted laser desorption/ionization and desorption/ionization on porous silicon, Rapid Commun. Mass Spectrom. 18 (2004) 2811–2817.
[32] M.P. Napolitano, P.C. Kuo, J.V. Johnson, J. Arslanoglu, R.A. Yost, Tandem mass spectrometry of laser-reduced anthraquinones for painted works and dyed cultural artifacts, Int. J. Mass Spectrom. 421 (2017) 14–24.
[33] M.V. Kosevich, O.A. Boryak, V.V. Orlov, V.S. Shelkovsky, V.V. Chagovets, S. G. Stepanian, V.A. Karachevtsev, L. Adamowicz, Evaluation of the reduction of imidazophenazine dye derivatives under fast-atom-bombardment mass-spectrometric conditions, J. Mass Spectrom. 41 (2006) 113–123.
[34] B. Tian, Z. Ding, G.H. Ning, W. Tang, C. Peng, B. Liu, J. Su, C. Su, K.P. Loh, Amino group enhanced phenazine derivatives as electrode materials for lithium storage, Chem. Commun. 53 (2017) 2914–2917.
[35] M. Gaberscek, M. Küzma, J. Jamnik, Electrochemical kinetics of porous, carbon-decorated $LiFePO_4$ cathodes: separation of wiring effects from solid state diffusion, Phys. Chem. Chem. Phys. 9 (2007) 1815–1820.